RESEARCH ARTICLE

Improved background oriented schlieren imaging using laser speckle illumination

Alexander H. Meier · Thomas Roesgen

Abstract A new variant of the background oriented schlieren technique is presented. Using a laser to generate a speckle reference pattern, several shortcomings of the conventional technique can be overcome. The arrangement decouples the achievable sensitivity from the placement constraint on the reference screen, facilitating the design of compact, high-sensitivity configurations. A new dual-pass imaging mode is introduced which further improves system performance and permits focusing on the target scene. Examples are presented that confirm the theoretical predictions.

1 Introduction

The background oriented schlieren (BOS) technique has attracted considerable interest in recent years because of its ability to provide quantitative data on refractive index variations in flow fields. Following the initial publications (see, e.g., Dalziel et al. 2000; Richard and Raffel 2001; Meier 2002), recent publications have focused on the accurate modeling (Goldhahn and Seume 2007) and validation (Elsinga et al. 2004) of the technique, but the basic concept has not undergone many changes or improvements.

In the present study, we introduce laser-projected speckle patterns as a synthetic background structure. Similar arrangements have been presented by Köpf (1972) and Debrus et al. (1972). These systems were limited to the detection of small refractive index variations, relying on an analysis of interference fringe patterns. Wernekinck and

Merzkirch (1987) improved the configuration to measure larger refractive index variations, and more recently, Hirahara and Kawahashi (1997) used this setup to measure the density field in supersonic flows. Nevertheless, the physical properties of the speckles were not fully utilized in these studies, despite the significant impact on the overall design of a BOS system and its sensitivity. A simple theoretical model is derived to explain the modified optical behavior, and experimental results are presented that confirm the predicted improvements in system performance.

2 Method

2.1 Generic BOS imaging model

In order to understand the working principle and limitations of a "standard" BOS system, we follow the description and geometrical definitions introduced in Goldhahn and Seume (2007), restricting the further analysis to small deflection angles α for clarity.

The observable pattern shift $\vec{\delta}$ on the sensor surface is linked to a ray deflection $\tan \vec{\varepsilon}$ across the test section by the simplified relationship

$$\vec{\delta} = Ml \tan \vec{\varepsilon}; \quad M = \frac{f}{l + m - f} \tag{1}$$

where f describes the focal length of the imaging lens, m the distance between lens and the test section, and l the separation between the test section and the background pattern onto which the lens is focused. The factor M represents the magnification of the lens imaging system. Newly introduced in this model is the distance s between the test section and the position of the *physical* scattering screen for the speckle illumination.

A. H. Meier (✉) · T. Roesgen
Institute of Fluid Dynamics, ETH Zurich, Zurich, Switzerland
e-mail: meier@ifd.mavt.ethz.ch

The observable shift $\vec{\delta}$ is maximized if the pattern distance becomes large and converges towards

$$\vec{\delta} \to f \tan \vec{\varepsilon} \qquad (2)$$

as $l \to \infty$. This figure describes the limiting sensitivity of a standard BOS system. It will be shown below that with a suitable speckle pattern, this limit can be exceeded.

2.2 Speckle characteristics

Speckle patterns are created when coherent light with a spatially random phase is interfering on a sensor surface. This is the case when the BOS reference pattern is replaced by a suitably roughened screen illuminated with laser light. Following the imaging model described in Goodman (2007), the autocorrelation of the speckle pattern in the sensing plane of a lens imaging system can be described as

$$\Gamma(r) = \bar{I}^2 \left[1 + \left| 2 \frac{J_1\left(\frac{\pi D r}{\lambda z}\right)}{\frac{\pi D r}{\lambda z}} \right|^2 \right] \qquad (3)$$

Here, λ is the laser wavelength, D the diameter of the imaging system's exit pupil, and z the distance between the imaging lens and the sensor plane. The radial coordinate in the sensor plane is r, and $\bar{I}^2$ denotes the average squared illumination intensity. Following Goodman's arguments, this model does *not* include the object distance $l + m$ between the lens and the scattering plane. In effect, the imaging lens aperture itself is considered as the source of the speckle pattern, not the BOS reference screen.

For a uniformly illuminated speckle aperture, the size of the speckles can be computed from the normalized covariance function $c(\Delta x, \Delta y)$ as

$$c(\Delta x, \Delta y) = \frac{\Gamma(\Delta x, \Delta y) - \bar{I}^2}{\bar{I}^2};$$

$$A_c = \iint c(\Delta x, \Delta y) \mathrm{d}\Delta x \, \mathrm{d}\Delta y = \frac{4}{\pi} \left(\frac{\lambda z}{D} \right)^2 \qquad (4)$$

The size definition makes use of the speckle area A_c rather than a direct linear length scale. For large object distances $l + m \gg z$ one has for the imaging configuration of Fig. 1 $z \to f$ and thus

$$A_c \to \frac{4}{\pi} \left(\frac{\lambda f}{D} \right)^2 \qquad (5)$$

This implies that the speckle "diameter" $\Delta_s = \sqrt{4A_c/\pi}$ is solely determined by the laser wavelength and the imaging lens f-number $f/\# = f/D$. The size of the reference pattern features, i.e., the speckle size, can be adjusted independent of the imaging geometry. It is simply a
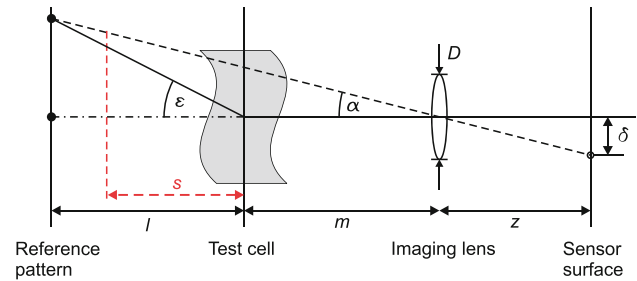
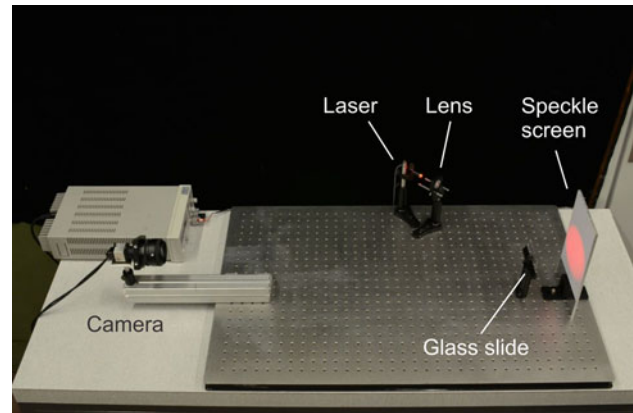**Fig. 1** Geometry of a generic BOS imaging system

Fig. 2 Experimental setup for testing BOS using speckle patterns (single pass configuration)

function of the imaging lens aperture size. (In a conventional BOS system, a compromise has to be found between sensor resolution, imaging distance, and pattern size.)

The camera can thus be focused at any position independent of the *physical* position of the reference screen, allowing to modify the *virtual* pattern distance l. The physical position s of the screen can be chosen close to the test cell without reducing sensitivity. (In a conventional BOS system, the overall sensitivity can only be increased by increasing f and/or l, approaching the limit described in Eq. (2).)

3 Experiments

3.1 Experimental configuration

Before various imaging configurations for the speckle-illuminated BOS system will be discussed in more detail, a brief description of the experimental is given.

The basic hardware configuration is shown in Fig. 2. A CCD camera (UI-2230, IDS Imaging Development Systems GmbH, pixel size 4.65 μm × 4.65 μm) with a F-mount lens (Nikon AF Nikkor 50 mm f/1.4D) was used to record images of the reference screen, here a simple white paper sheet. The distance $m + z$ between the sensor

plane and the distorting target was 945 mm, whereas the distance s between target and speckle screen was set at 100 mm.

The speckle patterns appearing on the sensor surface were created by a laser diode (Laser Components FP-64, $\lambda = 635$ nm, 10 mW) with a strong convex lens ($f = 6$ mm) to diffuse the beam. In order to maximize the apparent speckle size on the sensor, the lens was stopped down to $f/11$. A large conventional BOS screen (random dot pattern printed on a A0 format poster) could be positioned at variable distances $l > s$ behind the target.

The target distortions were created by the thickness variations in a standard $1'' \times 2''$ microscope glass slide. Using other, calibrated optical targets such as wedge prisms proved difficult because of the very high sensitivity of some of the BOS configurations to be tested.

Images were analyzed using the PIV algorithm as implemented in the commercial software package PIV-view2C (PIVTEC GmbH, Germany).

3.2 Regular BOS setup with speckle illumination

In this configuration, the position s of the speckle screen is fixed, while the camera focuses at a distance l. Two types of distortion patterns can be compared. If the speckle screen is inserted into the field of view of the camera, an apparent shift is detected in the speckle pattern between the distorted and target-free images. If the speckle screen is replaced by a standard BOS reference screen placed at the distance l, identical pattern shifts are extracted.

This result is quantified in Fig. 3, where the pattern shifts in an identical area of the target slide are compared for the stan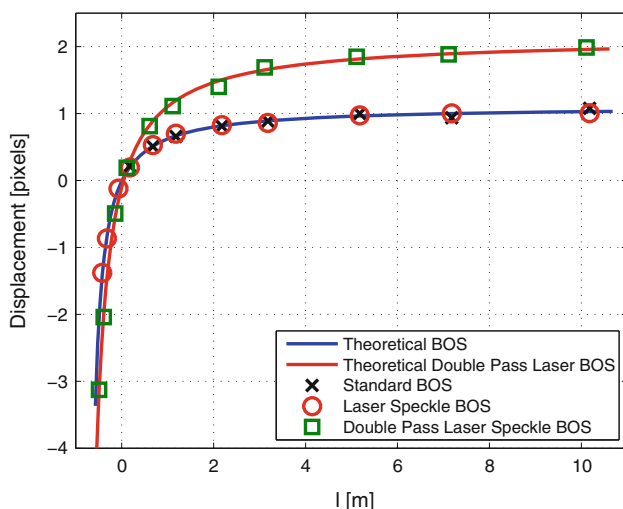dard (black symbols) and speckle based (red symbols) BOS configurations. Also shown is the theoretical curve (blue line) as derived from (1).

The measured displacement reaches an asymptotic value

$$\vec{\delta} = \frac{lf}{l + m - f} \tan \vec{\varepsilon} \quad \underset{l \to \infty}{\longrightarrow} \quad f \tan \vec{\varepsilon} \qquad (6)$$

for large pattern distances l and goes to zero as the focus distance behind the target becomes small.

The complete equivalence of the speckle and conventional screens is directly shown in Fig. 4, where the camera view is shown for a split scenery. The top half of the image shows the conventional reference screen placed at a large distance $l = 11$ m. In the bottom half, the speckle pattern produced by the scattering screen placed at $l = 100$ mm is recorded. The image is created simultaneously with the camera focused on the conventional BOS screen. The speckle screen is out-of-focus, but the imaged speckle pattern appears sharp as predicted by theory. As a distortion target, a burning candle is placed below the field of view.

The displacement vector field produced by a standard cross-correlation analysis is superimposed on the pattern image. The analysis is indiscriminate regarding the nature of the apparent displacements in the top and bottom halves of the image. The results are identical in the conventional and speckle regions of the BOS image, confirming the interchangeability of both types of background pattern for the same lens focus setting.

The advantage of the speckle setup is obvious. The limiting sensitivity can be reached without the need for large observation distances and the scattering screen can be placed very close to the distorting target without losing sensitivity.
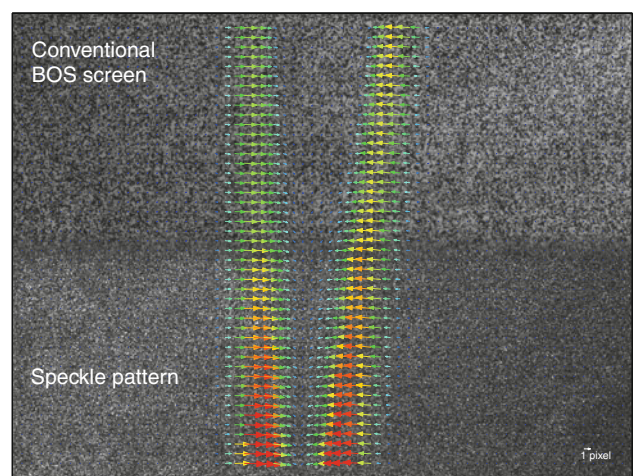

Fig. 3 Displacement as function of the lens imaging distance for conventional and speckle BOS measurements

Fig. 4 Burning candle plume imaged simultaneously with a conventional (*top*) and speckle (*bottom*) BOS reference pattern. Superimposed is the displacement vector field computed with a cross-correlation algorithm

3.3 Enhanced BOS imaging with negative focus distance

In the speckle configuration, the camera can also be focused *in front* of the distorting target, which is impossible with a conventional screen. This opens up a completely new imaging regime for BOS with increased sensitivity. Referring to Fig. 1, the virtual reference plane is now placed in the range $0 > l > -m + f$. Following Eq. (1), the observable displacement changes from zero ($l = 0$, virtual pattern/focus in the target plane) to a value becoming arbitrarily large as $l \rightarrow -m + f$. There is also a sign change in the observed displacement in this region. The quantitative exploration of this regime is also shown in Fig. 3 (red symbols for $l < 0$).

3.4 Double-pass BOS imaging

So far, the results were obtained by illuminating the speckle screen from the side (see Fig. 1), that is, without the incident laser beam passing directly through the distortion field. If the laser illumination is performed in-line (coaxially) with the camera view, another sensitivity increase can be achieved. Such an arrangement is shown in Fig. 5, where the speckle-generating laser beam is inserted into the camera's line of sight using total reflection from a suitably tilted glass plate. This helps to avoid multiple reflections from optical surfaces which would create spurious interference patterns otherwise.

Following the model for speckle interferometry (Debrus et al. 1972), the BOS Eq. (1) has to be expanded to include the incident laser beam deflection,

$$\vec{\delta}_{\parallel} = M l \, \tan \vec{\varepsilon} + M(l - s) \, \tan \vec{\varepsilon} = M(2l - s) \, \tan \vec{\varepsilon};$$
$$M = \frac{f}{l + m - f} \tag{7}$$

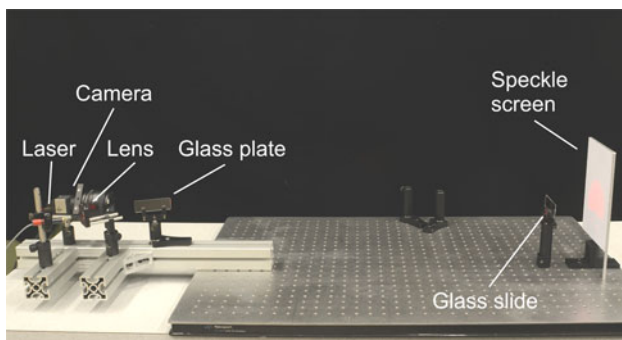Now the limiting sensitivity in the case $l \gg s > 0$ becomes

$$\vec{\delta}_{\parallel} = \frac{2l - s}{l + m - f} f \, \tan \vec{\varepsilon} \quad \underset{l \rightarrow \infty}{\rightarrow} \quad 2f \, \tan \vec{\varepsilon} \tag{8}$$

Again, the experimental results are included in Fig. 3 (green symbols) and confirm the model prediction of Eq. (7) (Fig. 3, orange line).

3.5 Speckle imaging with in-focus target

Finally, it is instructive to operate the speckle BOS setup as a speckle interferometer (see, e.g., Debrus et al. 1972; Fomin 1998). In the extended model for in-line illumination Eq. (7), this corresponds to setting $l = 0$, that is, an arrangement where the camera is focused onto the distortion target. The measurable displacement becomes

$$l = 0: \quad \vec{\delta} = -Ms \, \tan \vec{\varepsilon}; \quad M = \frac{f}{m - f} \tag{9}$$

which can be increased arbitrarily by moving the speckle screen to large distances behind the distorting target. Experimental confirmation of this behavior is shown in Fig. 6 where a burning lighter is imaged in the "interferometry mode" with a speckle screen distance $s = 750$ mm.

Using this configuration, one of the main drawbacks of regular BOS imaging is avoided: In regular BOS—also when using laser speckle illumination—the sensitivity is increased by defocusing the camera away from the schlieren object. Therefore, the sharpness of the schlieren object is reduced. In the "interferometry mode," the schlieren object can be kept in focus while increasing the sensitivity by placing the speckle screen farther from the target.
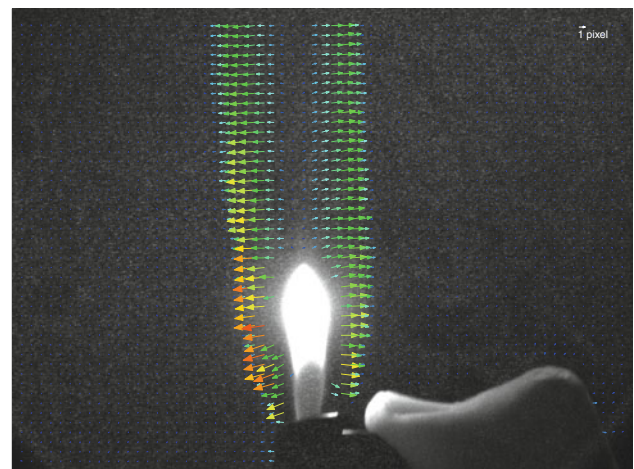

Fig. 5 Experimental setup for testing BOS using speckle patterns (double-pass configuration)

Fig. 6 Focused imaging using the speckle interferometer configuration (result vectors superimposed on raw image)

4 Implementation details

As indicated by Eq. (5), the size of the speckles is determined by the f-number of the imaging system and is thus primarily a function of the lens aperture size. Using representative values ($\lambda = 635$ nm, $f/D = 2.8$) the speckle size is according to Eq. (5) $\Delta_s \approx 2.3 \times 10^{-6}$ m which is comparable to and possibly less than a typical camera's pixel size (see also Lehmann 1997). Figure 7 shows a close-up of the speckle patterns recorded with four different f-numbers ranging from 1.4 to 11. At $f/\# = 1.4$, the speckle pattern shows a very fine structure. This structure becomes coarser by closing the aperture (i.e., increasing the f-number). As a consequence of the fine structure at small f-numbers, peak locking effects (Westerweel 2000) may become apparent during the displacement analysis.

The imaging lens aperture should therefore be chosen as small as possible to make the speckle size larger than the pixel size of the camera used. Figure 8 compares the measured displacements of the glass slide target for different f-numbers. The peak locking effect is clearly present at $f/\# = 1.4$ and 2.8, where an unphysical accumulation of measured displacements at integer y-shifts can be observed. Closing the aperture of the lens to $f/\# = 11$ results in a more even distribution of the measured displacements.

All experiments presented above were performed with an aperture setting of $f/11$, which represents a compromise between increased speckle size and the requirement for enough light to reach the sensor surface.

The image displacement models (Eqs. 1, 7) introduced above are valid strictly only close to the centerline of the imaging system. An extension of (1) for larger fields of view is given in Goldhahn and Seume (2007). The extension of the double-pass equation for large fields of view is trivial as the divergence of the illumination has no influence on the speckle interferometer performance (see Debrus et al. 1972). Therefore, again, only the part stemming from the BOS equation needs to be adapted.

A possible drawback of the speckle illumination BOS technique is its sensitivity to vibrations and relative motions between the camera and the scattering plane which is a consequence of the interferometric nature of the speckles. Small vibrations can be averaged by using a longer integration time of the camera leading to a somewhat blurred image of the speckles. Relative motions will no longer lead to a simple constant offset in the displacement field and may be difficult to detect and correct. For example, a tilt of the speckle screen between the two exposures leads to a linear increase in the apparent pattern displacement across the image.

In the present study, a simple white paper sheet was used as a scattering screen but other surfaces will also be suitable for the creation of speckles. In particular, micro-structured retro-reflecting screens were successfully
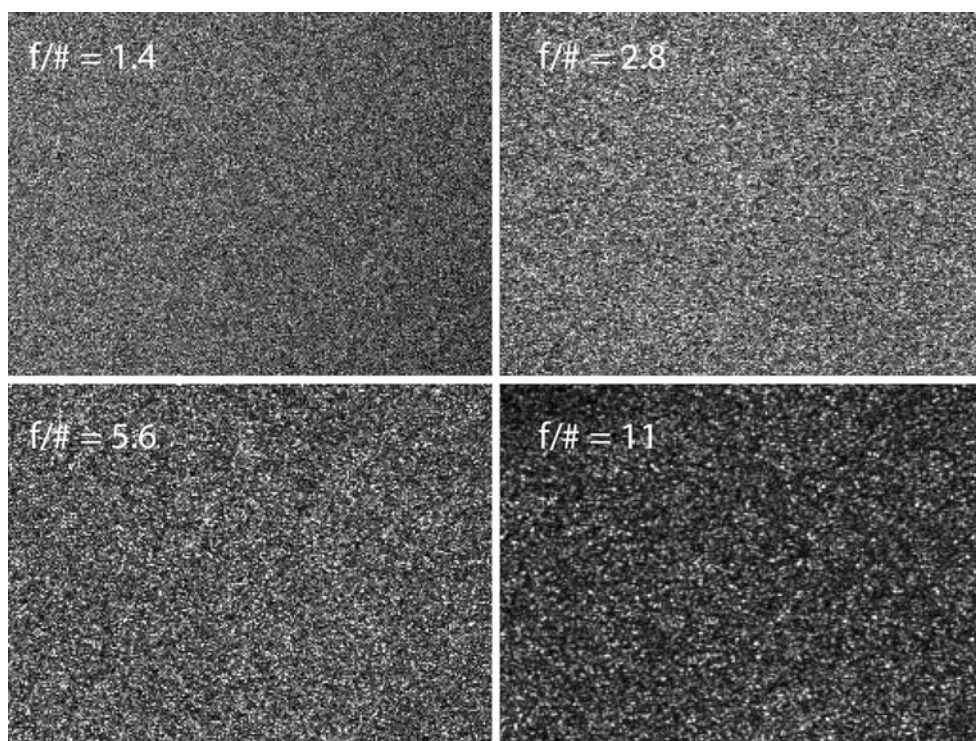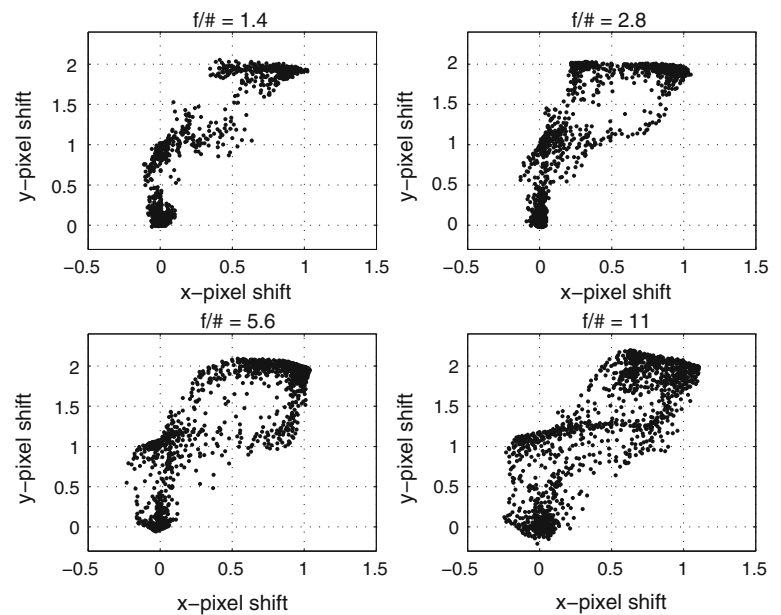

Fig. 7 Effect of the lens f-number on the speckle patterns

Fig. 8 Effect of lens *f*-number on peak locking in the displacement analysis

evaluated. Since they significantly reduce the requirements regarding the laser power, they may be well suited for large-scale geometries. Furthermore, the experiments by Erbeck and Merzkirch (1988) show that pulsed lasers can be used in speckle interferometry. It can therefore be expected that this will also work for the present technique, enabling time-resolved recordings in unsteady flow fields.

5 Conclusion

A new variant of the BOS technique is proposed which uses laser-generated speckle patterns as the background image to be analyzed. The advantage is an increase in the maximum achievable sensitivity and the possibility to place the physical reference screen close to the test section/distortion volume without compromising system performance. Furthermore, a focused target scene is possible when operating the BOS system as an in-line speckle interferometer.

References

Dalziel SB, Hughes GO, Sutherland BR (2000) Whole-field density measurements by 'synthetic schlieren'. Exp Fluids 28:322–335

Debrus S, Françon M, Grover CP, May M, Roblin M (1972) Ground glass differential interferometer. Appl Opt 11(4):853–857

Elsinga GE, van Oudheusden BW, Scarano F, Watt DW (2004) Assessment and application of quantitative schlieren methods: calibrated color schlieren and background oriented schlieren. Exp Fluids 36:309–325

Erbeck R, Merzkirch W (1988) Speckle photographic measurement of turbulence in an air stream with fluctuating temperature. Exp Fluids 6:89–93

Fomin NA (1998) Speckle photography for fluid mechanics measurements. Springer, Berlin

Goldhahn E, Seume J (2007) The background oriented schlieren technique: sensitivity, accuracy, resolution and application to a three-dimensional density field. Exp Fluids 43:241–249

Goodman JW (2007) Speckle phenomena in optics: theory and applications. Roberts & Company, Englewood

Hirahara H, Kawahashi M (1997) Density field measurement of mach reflection of shock waves by laser speckle method. Proc SPIE 3172:238–245

Köpf U (1972) Application of speckling for measuring the deflection of laser light by phase objects. Opt Comm 5(5):347–350

Lehmann M (1997) Measurement optimization in speckle interferometry: the influence of the imaging lens aperture. Opt Eng 36(4):1162–1168

Meier GEA (2002) Computerized background-oriented schlieren. Exp Fluids 33:181–187

Richard H, Raffel M (2001) Principle and applications of the background oriented schlieren (BOS) method. Meas Sci Technol 12:1576–1585

Wernekinck U, Merzkirch W (1987) Speckle photography of spatially extended refractive-index fields. Appl Opt 26(1):31–32

Westerweel J (2000) Effect of sensor geometry on the performance of PIV interrogation. In: Adrian RJ et al (eds) Laser techniques applied to fluid mechanics. Springer, Berlin, pp 37–55